GEOPHYSICAL RESEARCH LETTERS, VOL. 32, XXXX, DOI:10.1029/2005GL023588,

Rupture processes of the 2004 Chuetsu (mid-Niigata prefecture) earthquake, Japan: A series of events in a complex fault system

Kazuhito Hikima

Earthquake Research Institute, University of Tokyo, Tokyo, Japan

Technical Center, OYO Corporation, Saitama, Japan

Kazuki Koketsu

Earthquake Research Institute, University of Tokyo, Tokyo, Japan

Kazuhito Hikima, Earthquake Research Institute, University of Tokyo, 1-1-1 Yayoi, Bunkyo-ku, Tokyo, 113-0032, Japan. (hikima@eri.u-tokyo.ac.jp)

We relocated the hypocenters of the 2004 Chuetsu earthquake sequence, Niigata, Japan, using the double-difference method. The distribution of aftershocks reveals a complex fault system consisting of five different fault planes. Inversions of strong motion records for the five major events within the sequence indicate that the mainshock (M_{W} 6.6) and the largest aftershock (M_{W} 6.3) occurred on parallel WNW-dipping fault planes. The zones of large slip (asperities) of these two events are located near the hypocenters. In contrast, the three other large earthquakes (M_W 5.9, 5.7 and 5.9) occurred on east-dipping fault planes oriented perpendicular to the fault plane of the mainshock. We used slip distributions deduced from waveform inversions to estimate the Coulomb failure stress changes that occurred immediately prior to each event. ΔCFF values were positive at the hypocenters and within the asperities of the major aftershocks. These results suggest that stress changes resulting from individual earthquakes led directly to the occurrence of subsequent earthquakes within the complex fault system.

1. Introduction

An earthquake of JMA magnitude (M_{JMA}) 6.8 occurred in the Chuetsu region of Niigata prefecture, central Japan at 17:56 on October 23, 2004 (JST=UT+9 hours) [*JMA*: Japan Meteorological Agency, 2005]. This mainshock was followed by vital aftershock activities, and the number of large aftershocks was significantly greater than recent crustal earthquakes in Japan [JMA, 2005]. The four especially large aftershocks occurred at 18:03 (M_{JMA} 6.3), 18:11 (M_{JMA} 6.0) and 18:34 (M_{JMA} 6.5) on October 23, and at 10:40 on October 27 (M_{JMA} 6.1). The mainshock and four $M6$ aftershocks of the earthquake sequence represent a series of five events within a single fault system (Figure 1).

Despite the moderate magnitude of the earthquakes, the seismic sequence resulted in 46 deaths, 4,301 injuries, the destruction of 2,827 houses [*FDMA*: Fire and Disaster Management Agency, 2005] and thousands of landslides [*Sidle et al.*, 2005]. *Kato et al.* [2005] investigated the velocity structure of the source region of the earthquakes and the geometry of the fault system in order to understand the cause of the earthquake sequence. This study also pursues the cause by determining the accurate geometry of the fault system. We relocate the hypocenters of the major events and smaller aftershocks, and use these data to determine candidate fault planes. We will then perform the inversions of strong motion records to determine the fault planes and the rupture processes of the major events. Finally, we use fault geometry and slip distributions to calculate changes in static stress, and we discuss the nature of interaction between the five major events.

2. Aftershock Distribution

The accurate location of aftershock hypocenters within the Chuetsu earthquake sequence is an important clue to the geometry of the fault plane of the mainshock [e.g., *Page*, 1968]. The Seismological and Volcanological Bulletin of Japan [*JMA*, 2005] provides a reliable catalog of hypocenter data for earthquakes in Japan, but the locations described in this bulletin contain a bias toward the southeast because of the highly irregular velocity structure within the source region [*Kato et al.*, 2005]. We have used the double-difference (DD) method [*Waldhauser and Ellsworth*, 2000] with arrival time data published in the bulletin to relocate the hypocenters of the major events and smaller aftershocks of the Chuetsu seismic sequence. Because the DD method can determine not only the relative positions but also the absolute locations of aftershocks, overcoming unmodeled heterogeneity of velocity structure [*Menke and Schaff*, 2004], it was suitable for the relocation of these events.

The depth profile of the aftershock distribution suggests activity upon five distinct fault planes (Figure 2). We determined the orientations of the plane referring to the focal solutions provided by *NIED* (National Research Institute for Earth Science and Disaster Prevention) [2004]. The mainshock (event 1) and largest aftershock (event 4) are located on parallel westward-dipping planes (planes A and D respectively). Event 5 is located on

plane E oriented perpendicular to planes A and D. The orientations of the fault planes related to events 2 and 3 are less easily determined. The hypocenter of event 3 is close to that of event 1, but appears to be located on a poorly defined plane (plane C) oriented perpendicular to plane A. A second poorly defined plane (plane B) oriented perpendicular to planes A and D contains event 2. Therefore, all events should have had different fault planes, if rupture process inversions confirm that event 2 and 3 occurred on planes B and C, respectively.

3. Rupture Process Inversions

We used three-component seismograms recorded by borehole instruments at eleven KiK-net stations [*Aoi et al.*, 2000; Figure 1] to perform the rupture process inversion. Borehole data were chosen to avoid site effects related to shallow soil conditions. The observed accelerograms were numerically integrated to obtain velocity waveforms. The resultant velocities were filtered out with a pass band of 0.02 – 0.5 Hz and re-sampled with an interval of 0.2 s. We used the reflectivity method of *Kohketsu* [1985], with an extension to buried receivers [*Koketsu et al.*, 2004], to calculate the Green's functions for borehole seismograms.

In order to obtain accurate Green's functions, we used an inverse scheme similar to that described by *Ichinose et al.* [2003] to determine a set of one-dimensionally stratified velocity models adapted to each station. The seismograms from the moderate magnitude aftershock (M_{W} 5.0) at 18:57 on October 23 were inverted with fixed point source parameters and layer velocities. The initial model was constructed from the results of seismic explorations in central Japan [e.g., *Takeda et al.*, 2004]. The partial derivatives were calculated numerically by taking the differences between the synthetic seismograms for the initial model and those generated with 5% perturbations of a layer thickness. We then determined the layer thicknesses by an iterative non-linear inversion using the focal solution of the *NIED* [2004]. Figure S1 shows examples of the resultant velocity models and comparisons of the observed and synthetic seismograms. The models were validated by comparison with other aftershocks located near the mainshock.

The rupture process inversions followed the method of *Yoshida et al.* [1996], which is based on the formulation of multiple time windows. Slip orientation data indicate reverse faulting of these events [e.g., *NIED*, 2004]. Slip vectors are therefore represented by a linear combination of two components in the directions of 90±45°. Each component is constrained to a positive value using the non-negative least square algorithm of *Lawson and Hanson* [1974] rather than the penalty functions of *Yoshida et al.* [1996]. The inversion was subject to a smoothness constraint with a discrete Laplacian in space and time. The weight of the constraint was determined using ABIC [*Akaike*, 1980]. Although we constructed the set of adaptive 1-D velocity models ourselves, the models remain incomplete. To minimize artifacts resulting from the incomplete nature of the models,

scalar time shifts were added to the Green's functions, and the amounts of the time shifts were also determined by the inversion method of *Graves and Wald* [2001].

4. Fault Models and Slip Distributions

We use the fault planes shown in Figure 2 as fault models for analyzing slip distribution. Fault model orientations were derived from focal solutions provided by *NIED* [2004] and preliminary inversions of far-field body waves. We used the epicenter locations detailed in Figure 2 for determining the horizontal locations of initial rupture during the major events. The depths of these events were shifted slightly to minimize the residuals between the observed and synthetic waveforms. The fault models were divided into 2×2 km^2 subfaults and the slip histories were represented by a combination of ramp functions with a rise time of 1 s. As described earlier, it is difficult to identify the fault planes of events 2 and 3 from the aftershock distribution. To overcome this limitation, we performed rupture process inversions for planes B and C (Figure 2) and perpendicular planes, and chose the plane with the better fit. We measured the fit by both total residual and the partial residual at distinct phases in the near-source waveforms.

The most suitable orientation for the fault planes related to events 2 and 3 is that of planes B and C, perpendicular to the fault planes of the mainshock and largest aftershock (Figure S2), dipping to the east. The rupture process inversions confirm that the five major events occurred on five different fault planes. All five fault planes strike in a NNE-SSW direction (Figure 3), but two of the planes dip westward while the other three dip eastward. The parameters of these fault planes are summarized in Table 1.

All rupture process inversions produced sound results, as evident in waveform comparisons of the mainshock and largest aftershock (Figure S3). Figure 3 also shows slip distributions projected onto the ground surface. Rupture associated with the mainshock initiated from a deep part of the fault plane, and large slips occurred about the hypocenter. A maximum slip of about 1.7 m was recorded several kilometers to the north of the hypocenter (Figure 3a), suggesting that the direction of rupture propagation was dominantly northward. The asperity of the largest aftershock is also centered about the hypocenter and recorded a maximum slip of about 1.0 m. The rupture propagated to the south and the slip distribution is more complex than that of the mainshock (Figure 3b). The other events have relatively simple slip distributions consisting of a single asperity around the hypocenter (Figure 3c).

5. Discussion and Conclusions

To assess the nature of any interaction among the major events, we calculated static Coulomb failure stress change (ΔCFF) using the recovered slip distributions. We used the formula of *Okada* [1992], assuming the fault system to be buried in a homogeneous halfspace with an apparent frictional coefficient of 0.4. The receiver faults were set ac-

cording to the geometry described in Table 1 and assuming pure reverse faulting. Figure 4 shows the distribution of ΔCFF immediately prior to the largest aftershock (event 4) and following events 1, 2 and 3 on a horizontal plane at the depth of the hypocenter of event 4. The ΔCFF is positive around the future site of the event 4 hypocenter and asperity as imaged from the horizontal and vertical distributions of ΔCFF in Figure 4. Positive ΔCFF values in the range 0.03 – 0.28 MPa were also determined for the hypocenters of the other major aftershocks for the time period immediately prior to rupture (Figure S4). Although the association of positive ΔCFF and aftershock activity has been previously reported [e.g., *Reasenberg and Simpson*, 1992; *Harris*, 1998], the majority of such studies describe aftershocks far from the area of the mainshock. Figures 4 and S4 show that interaction among moderate magnitude closely located aftershocks can be explained by reference to ΔCFF values calculated from recovered slip distributions. The positive ΔCFF values calculated about the hypocenters for the time immediately prior to rupture suggests that the major aftershocks were triggered by stress changes caused by preceding events.

The 2004 Chuetsu earthquake sequence is characterized by the large number of large aftershocks. 46 events of JMA magnitude 4.5 or greater occurred in the month following the mainshock [*JMA*, 2005]. In contrast, the 1995 Kobe earthquake (M_{W} 6.9) and the 2000 western Tottori earthquake (M_{W} 6.7) generated only 13 and 8 aftershocks respectively of M_{JMA}4.5 or greater. *Yamanaka and Shimazaki* [1990] examined the linear scaling of aftershock numbers with respect to the seismic moment of crustal earthquakes in Japan. According to their scaling model, the Chuetsu earthquake should have produced only 9 aftershocks with the mainshock and largest aftershock moments of 1.2×10^{19}Nm. *Yamanaka and Shimazaki* [1990] concluded that aftershocks occur within areas of high strength on the mainshock fault that failed to rupture during the mainshock event. The aftershocks of the Chuetsu earthquake occurred on the mainshock fault and four other nearby faults. We consider the disparity in predicted and actual aftershock numbers related to the Chuetsu earthquake to be directly related to the occurrence of aftershocks on multiple fault planes.

We determined the fault geometry and rupture processes for the five major events of the 2004 Chuetsu earthquake sequence using strong motion records, hypocenters relocated using the DD method, and calibrated one-dimensionally stratified velocity models. We conclude that the five major events occurred on five different fault planes. The ΔCFF due to prior events was positive around the major aftershocks.

The source region of the earthquakes contains complex geological structures and numerous faults and cracks [*Kato et al.*, 2005] related to past tectonic activities [*Sato*, 1994]. High strain rates have been also recorded in this region [*Sagiya et al.*, 2000]. These features of the tectonic setting controlled the occurrence of the mainshock. The mainshock caused changes in the local stress distribution that triggered large aftershocks. Each af-

tershock also had an effect upon the stress distribution and influenced the occurrence and location of subsequent aftershocks.

Acknowledgments. We thank NIED for the strong motion records from KiK-net and the mechanism solutions from F-net. We are also grateful to JMA *et al.* for the hypocenter list and arrival time data. Thoughtful comments from two anonymous reviewers improved this manuscript. We thank Drs. Waldhauser, Wessel and Smith for the hypoDD and GMT codes. Drs. S. Sakai and A. Kato provided valuable suggestions and discussion. This study was supported by the DaiDaiToku Project I and the Grant-in-Aid for Scientific Research No. 15540403 from MEXT of Japan.

References

Akaike, H. (1980), Likelihood and Bayes procedure, in *Bayesian Statistics*, edited by J. M. Bernardo *et al.*, pp. 143-166, Univ. Press, Valencia, Spain.

Aoi, S., K. Obara, S. Hori, K. Kasahara, and Y. Okada (2000), New strong-motion observation network: KiK-net, *Eos Trans. AGU*, *81 (48)*, Fall Meet. Suppl., Abstract S71A-05.

FDMA (2005), *The 2004 Chuetsu, Niigata, earthquake (No. 66)*, http://www.fdma.go.jp/data/010502221022317478.pdf.

Graves, R. W., and D. J. Wald (2001), Resolution analysis of finite fault source inversion using one- and three-dimensional Green's functions 1. Strong motions, *J. Geophys. Res.*, *106*, 8745-8766.

Harris, R. A. (1998), Introduction to special section: Stress triggers, stress shadows, and implications for seismic hazard, *J. Geophys. Res.*, *103*, 24347-24358.

Ichinose, G. A., H. K. Thio, P. G. Somerville, T. Sato, and T. Ishii (2003), Rupture process of the 1944 Tonankai earthquake (M_S8.1) from the inversion of teleseismic and regional seismograms, *J. Geophys. Res.*, *108*, doi:10.1029/2003JB002393.

JMA (2005), *The Seismological and Volcanological Bulletin of Japan for October 2004*, JMA, Tokyo.

Kato, A. *et al.* (2005), Imaging the source region of the 2004 mid-Niigata prefecture earthquake and the evolution of a seismogenic thrust-related fold, *Geophys. Res. Lett.*, *32*, doi:10.1029/2005GL022366.

Kohketsu, K. (1985), The extended reflectivity method for synthetic near-field seismograms, *J. Phys. Earth*, *33*, 121–131.

Koketsu, K., K. Hikima, S. Miyazaki and S. Ide (2004), Joint inversion of strong motion and geodetic data for the source process of the 2003 Tokachi-oki, Hokkaido, earthquake, *Earth Planets Space*, *56*, 329–334.

Lawson, C. L., and R. J. Hanson (1974), Solving Least Squares Problems, Prentice-Hall, Englewood Cliffs., N. J.

Menke, W., and D. Schaff (2004), Absolute earthquake locations with differential data, *Bull. Seismol. Soc. Am.*, *94*, 2254-2264.

NIED (2004), *Earthquake Mechanism Information*, http://www.fnet.bosai.go.jp/freesia/event/hypo/joho.h

Okada, Y. (1992), Internal deformation due to shear and tensile faults in a half-space, *Bull. Seismol. Soc. Am.*, *82*, 1018-1040.

Page, R. (1968), Aftershock and microaftershocks of the great Alaska earthquake of 1964, *Bull. Seismol. Soc. Am.*, *58*, 1131–1168.

Reasenberg, P. A., and R. W. Simpson (1992), Response of regional seismicity to the static stress change produced by the Loma Prieta earthquake, *Science*, *255*, 1687-1690.

Sagiya, T., S. Miyazaki, and T. Tada (2000), Continuous GPS array and present-day crustal deformation of Japan, *Pure Appl. Geophys.*, *38*, 2303-2322.

Sato, H. (1994), The relationship between late Cenozoic tectonic events and stress field and basin development in northeast Japan, *J. Geophys. Res.*, *99*, 22261-22274.

Sidle, R. C., T. Kamai, and A. C. Trandafir (2005), Evaluating landslide damage during the 2004 Chuetsu earthquake, Niigata, Japan, *EOS Trans. AGU*, *86(13)*, 133–136.

Takeda, T. *et al.* (2004), Crustal structure in the northern Fossa Magna region, central Japan, from refraction/wide-angle reflection data, *Earth Planets Space*, *56*, 1293–1299.

Yamanaka, Y., and K. Shimazaki (1990), Scaling relationship between the number of aftershocks and the size of the main shock, *J. Phys. Earth*, *38*, 305–324.

Yoshida, S. *et al.* (1996), Joint inversion of near- and far- field waveforms and geodetic data for the rupture process of the 1995 Kobe earthquake, *J. Phys. Earth*, *44*, 437–454.

Waldhauser, F., and W. L. Ellsworth (2000), A double-difference earthquake location algorithm: method and application to the Northern Hayward fault, California, *Bull. Seismol. Soc. Am.*, *90*, 1353-1368.

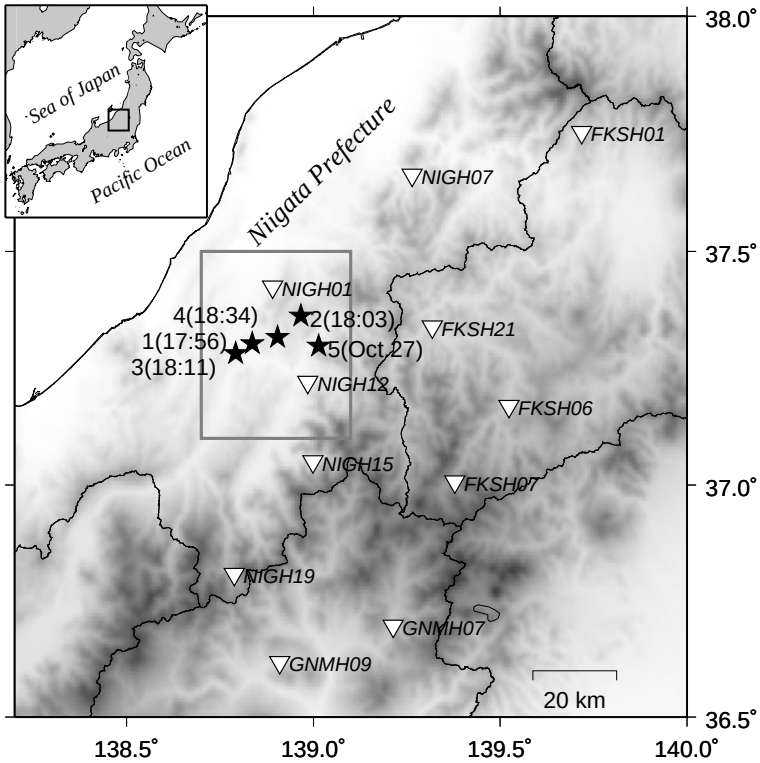

Figure 1. Location of the 2004 Chuetsu earthquake sequence. The rectangle indicates the target area of this study. Black stars represent the epicenters of the five major events. Chronological order and timing of rupture events is also indicated. Triangles represent KiK-net stations that recorded strong motion data analyzed in this study.

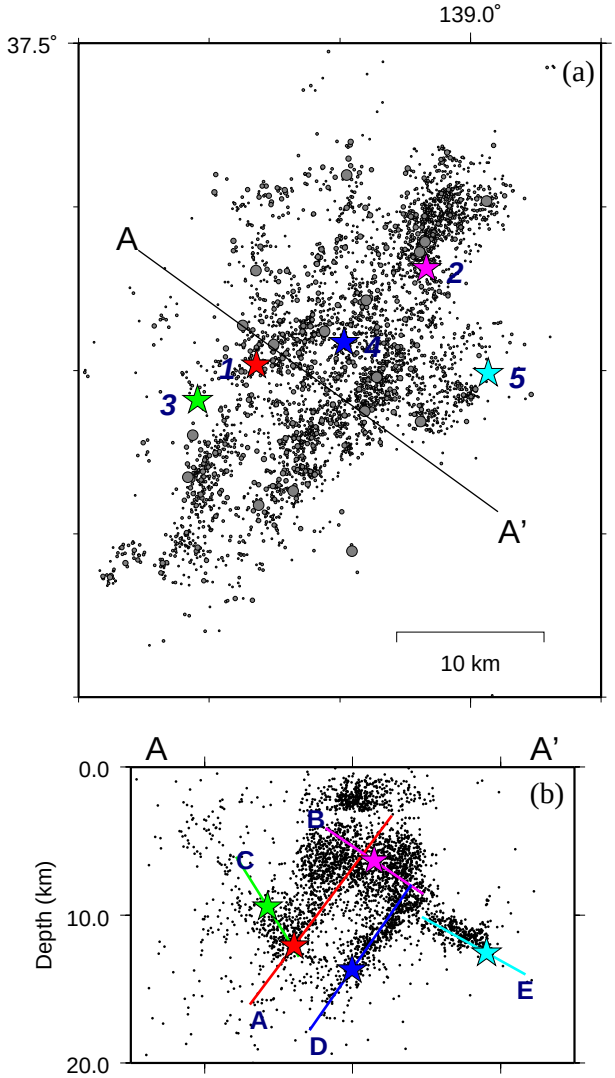

Figure 2. (a) Relocated epicenters of the major events (stars) and smaller aftershocks (circles). (b) Depth profile of hypocenters. The profile is oriented perpendicular to the strike of the mainshock fault plane (A-A'). The candidates of fault planes (color segments) were determined referring to *NIED* [2004].

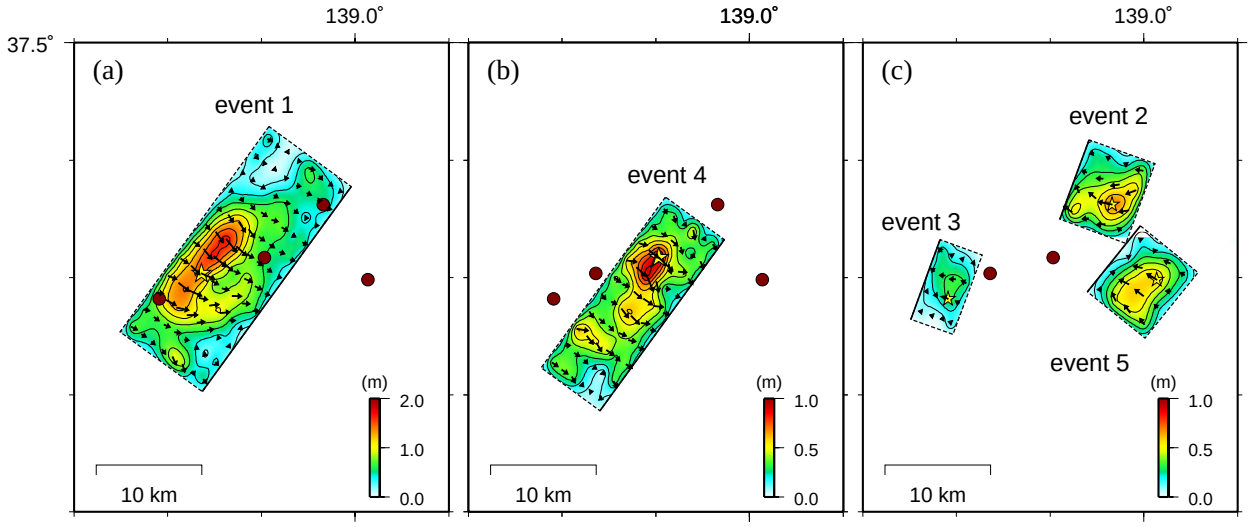

Figure 3. Surface projections of the recovered slip distributions for (a) the mainshock (event 1), (b) the largest aftershock (event 4) and (c) the other major aftershocks (events 2, 3 and 5). Yellow stars indicate the hypocenter locations of the relevant slip event. Brown dots represent the hypocenters of other events.

Table 1. Summary of Fault Parameters

No.	Date Time	Strike (°)	Dip (°)	Depth* (km)	M_{JMA}	M_{W}	M_{o} (Nm)
1	Oct.23 17:56	216	53	9	6.8	6.6	8.8×10^{18}
2	Oct.23 18:03	20	34	7	6.3	5.9	8.5×10^{17}
3	Oct.23 18:11	20	58	9	6.0	5.7	4.1×10^{17}
4	Oct.23 18:34	216	55	12	6.5	6.3	3.2×10^{18}
5	Oct.27 10:40	39	29	11.5	6.1	5.9	7.5×10^{17}

* Depth of hypocenter

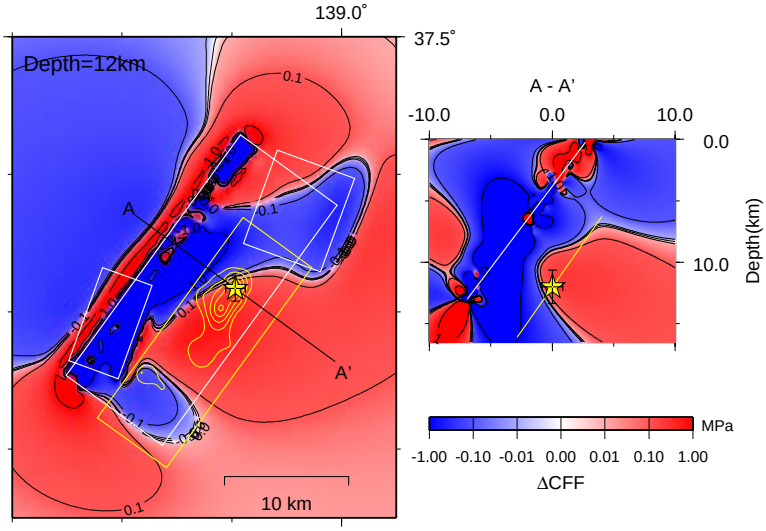

Figure 4. Distribution of ΔCFF resulting from events 1 – 3 (white rectangles) on a horizontal plane at the depth of the hypocenter of the largest aftershock (event 4). The zones of positive ΔCFF are shown in red. The hypocenter and fault plane are indicated by the yellow star and yellow rectangle respectively. Crosses indicate the error bars. Contours represent slip of > 0.5 m within the asperity. The right-hand figure is a cross-section along the line A-A'.

Auxiliary Material Submission for Paper 2005GL023588

Rupture processes of the 2004 Chuetsu (mid-Niigata prefecture) earthquake, Japan: A series of events in a complex fault system

Kazuhito Hikima (Earthquake Research Institute, University of Tokyo / OYO Corporation, Technical Center)

Kazuki Koketsu (Earthquake Research Institute, University of Tokyo)

Introduction

These figures are additional materials which we could not include in the paper. The examples of the inversion for one-dimensionally stratified velocity structures are shown in Figure S1. As the results of the rupture process inversions, the choise of fault plane is explained in Figure S2a-b and the comparisons of resultant waveforms are given in Figure S3a-b. Figure S4 shows the distributions of delta-CFF for the four aftershocks.

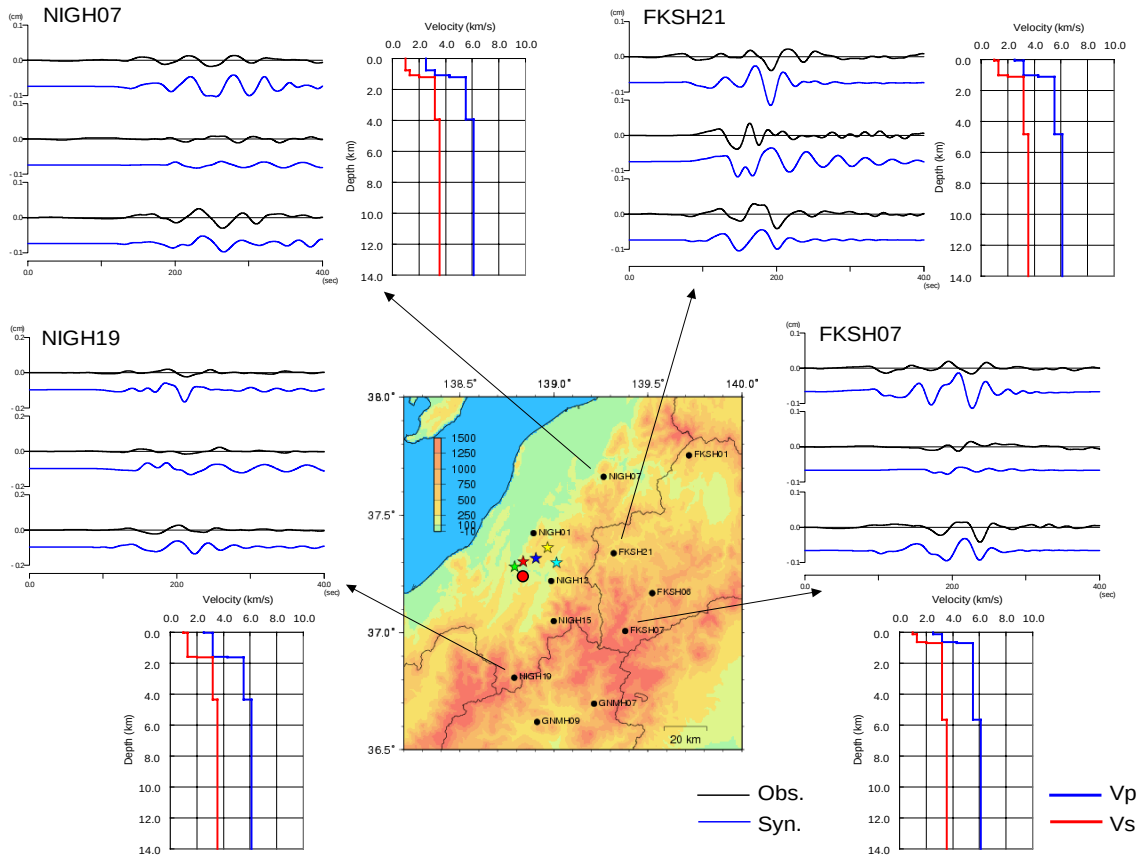

Figure S1 The one-dimensionally stratified velocity models obtained by the structural inversions for the four stations NIGH07, NIGH19, FKSH21, and FKSH07. The radial, transverse, and vertical components of the observed seismograms from an M5 aftershock (black traces) are compared with those of the synthetics for the final velocity models (blue traces). The depth profiles of P-wave and S-wave velocities represent the velocity models.

(a)

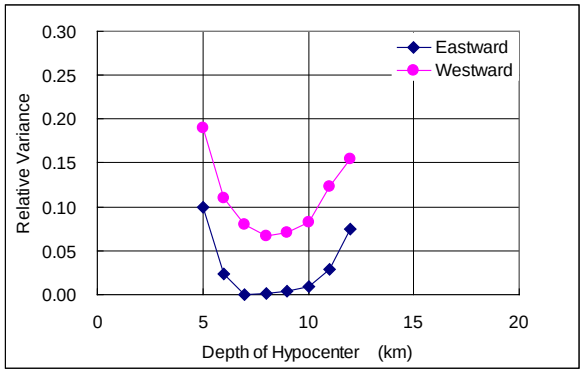

(b)

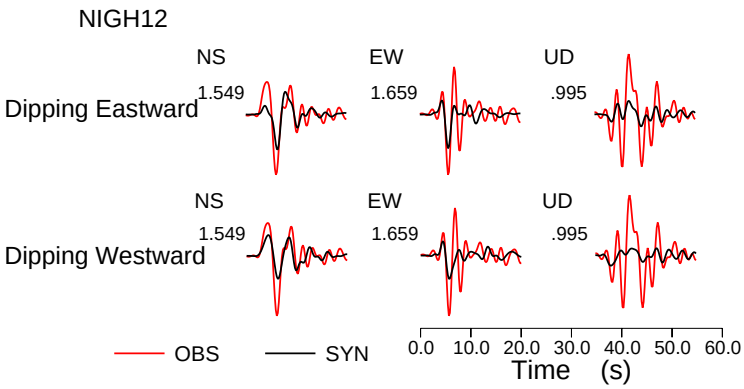

Figure S2a Figures S2a and S2b display the diagrams supporting the choices of fault planes for the events 2 and 3, respectively. (a) The comparison of the relative variances of the rupture process inversion results for the fault planes dipping eastward and westward. (b) The synthetic seismograms at the station NIGH12 for the optimum solutions for both the fault planes overlying the observed seismograms.

(a)

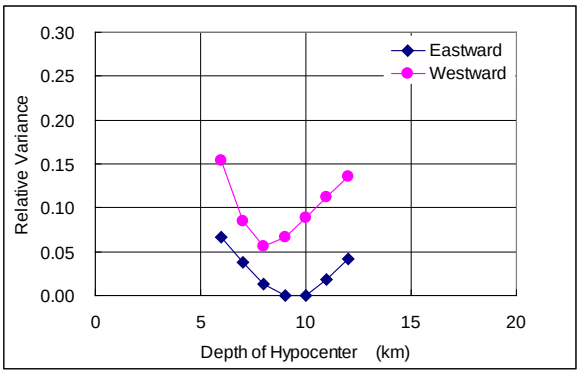

(b)

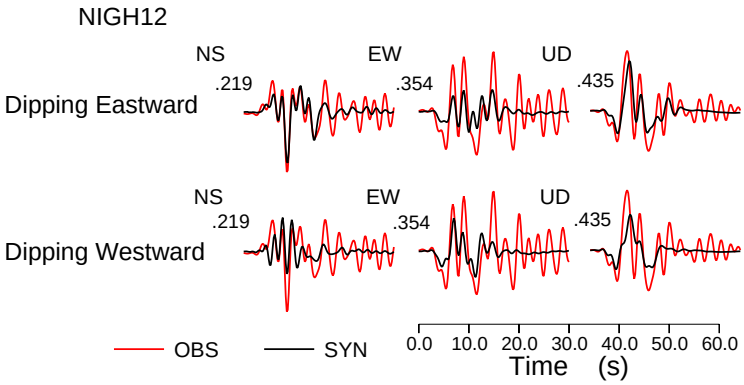

Figure S2b

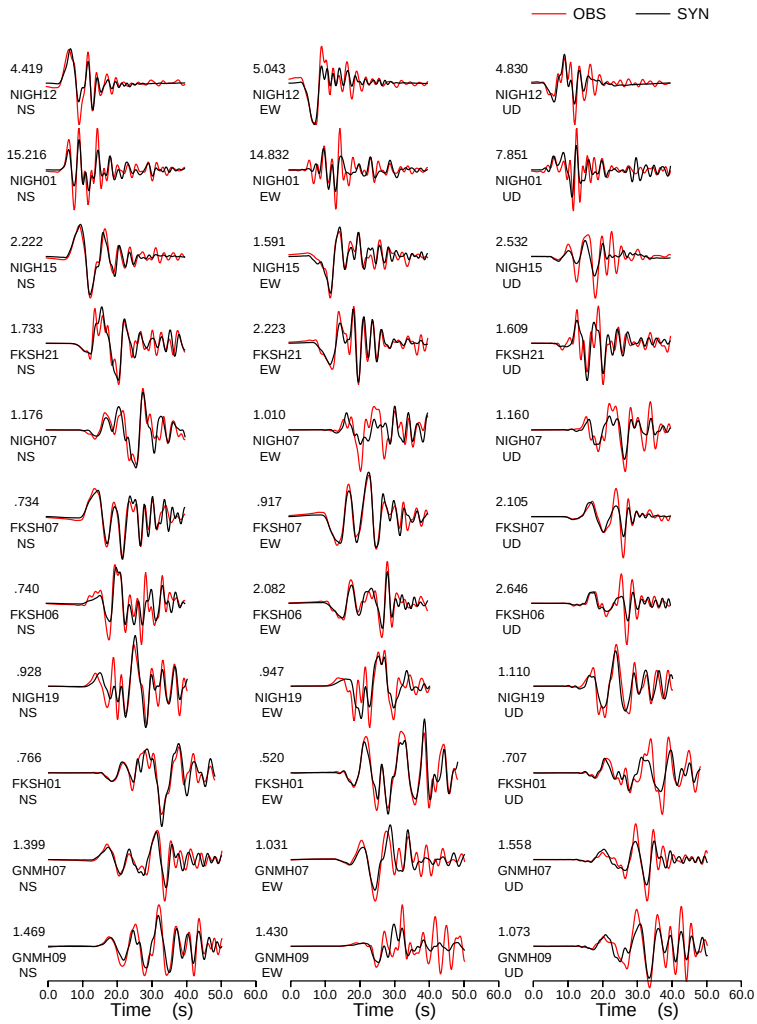

Figure S3a Comparisons between the observed (red) and synthetic (black) waveforms for the mainshock (event 1) and the largest aftershock (event 4). The rupture was initiated at 0 s. The figures above the stations codes represent the maximum velocities in cm/s.

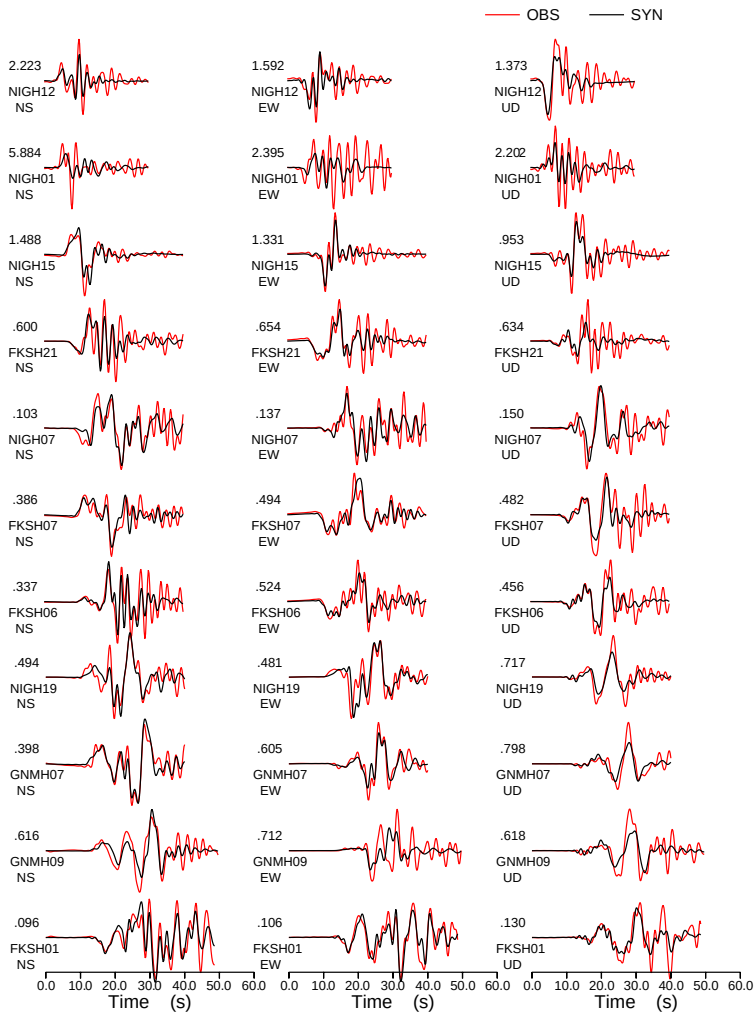
OBS
SYN
2.223
NIGH12
NS
1.592
NIGH12
EW
1.373
NIGH12
UD
5.884
NIGH01
NS
2.395
NIGH01
EW
2.202
NIGH01
UD
1.488
NIGH15
NS
1.331
NIGH15
EW
.953
NIGH15
UD
.600
FKSH21
NS
.654
FKSH21
EW
.634
FKSH21
UD
.103
NIGH07
NS
.137
NIGH07
EW
.150
NIGH07
UD
.386
FKSH07
NS
.494
FKSH07
EW
.482
FKSH07
UD
.337
FKSH06
NS
.524
FKSH06
EW
.456
FKSH06
UD
.494
NIGH19
NS
.481
NIGH19
EW
.717
NIGH19
UD
.398
GNMH07
NS
.605
GNMH07
EW
.798
GNMH07
UD
.616
GNMH09
NS
.712
GNMH09
EW
.618
GNMH09
UD
.096
FKSH01
NS
.106
FKSH01
EW
.130
FKSH01
UD
0.0 10.0 20.0 30.0 40.0 50.0 60.0
Time (s)

Figure S3b

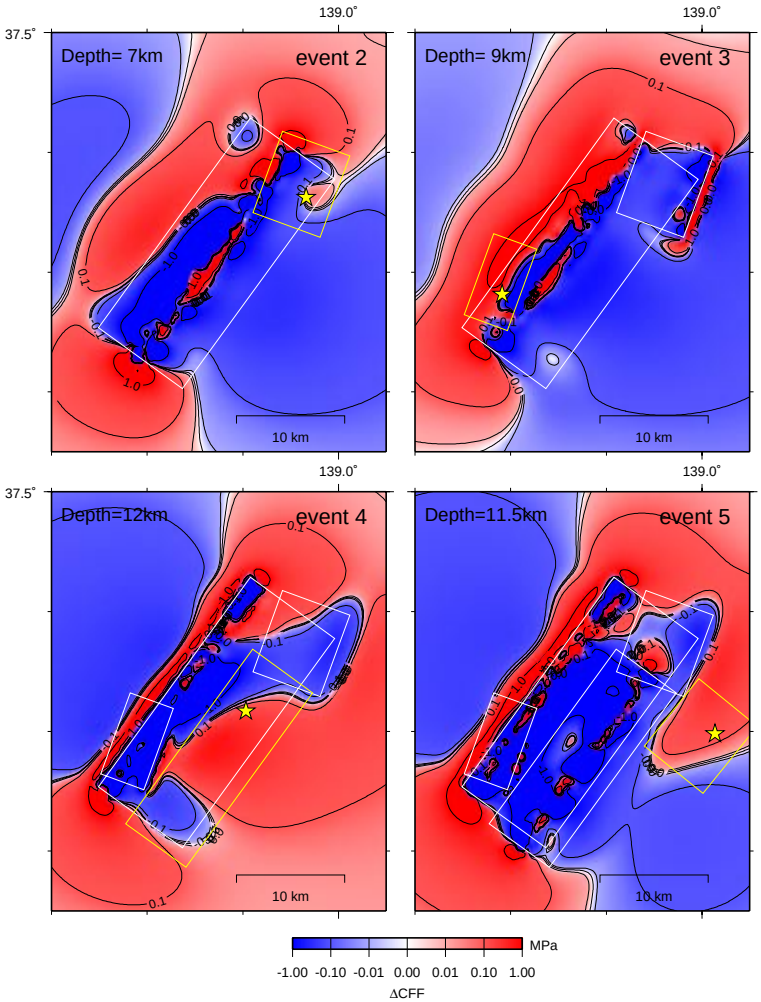

Figure S4 Distributions of delta-CFF on the horizontal planes at the depths of the hypocenters of the major aftershocks. The white rectangles denote the fault planes of the preceding events. The hypocenter and fault plane of a target event are shown by a yellow star and rectangle, respectively.